Evolution of Laterally Phase-Separated Polyfluorene Blend Morphology Studied by X-ray Spectromicroscopy

Christopher R. McNeill,*,† Benjamin Watts,‡,⊥ Lars Thomsen,§,∥ Warwick J. Belcher,§ Neil C. Greenham,† Paul C. Dastoor,§ and Harald Ade‡

Cavendish Laboratory, Department of Physics, University of Cambridge, J J Thomson Avenue, Cambridge CB3 0HE, United Kingdom; Department of Physics, North Carolina State University, Raleigh, North Carolina 27695; School of Mathematical and Physical Sciences, University of Newcastle, University Drive, Callaghan, NSW 2308, Australia; and Australian Synchrotron, 800 Blackburn Rd., Clayton, VIC 3168, Australia

Received August 8, 2008; Revised Manuscript Received March 9, 2009

ABSTRACT: The morphological evolution of laterally phase-separated polyfluorene blends composed of poly(9,9′-dioctylfluorene-*co*-bis-*N,N*′-(4-butylphenyl)-bis-*N,N*′-phenyl-1,4-phenylenediamine) (PFB) and poly(9,9′-dioctylfluorene-*co*-benzothiadiazole) (F8BT) has been studied with scanning transmission X-ray microscopy (STXM). The degree of phase separation in the films was regulated by controlling the time spent in a solvent-saturated atmosphere during solution processing, typically between 1 and 6 min. For films with a 5:1 weight ratio of PFB:F8BT, we observe a systematic increase in domain size and domain purity, with the enclosed F8BT-rich domains growing both through coalescence and flow of material across the domain boundary. For 1:1 and 1:5 blends a more complicated evolution of morphology is observed with evidence of additional vertical stratification. For 1:1 blends, primary and secondary phase separation is observed, with the evolution of the PFB-rich phase evolving similar to the 5:1 blend. Interestingly, the PFB-rich spots within the F8BT domain are observed to disappear after around 3 min of morphology evolution. Similar behavior is also seen in 1:5 blends, where a dramatic partial phase inversion is observed. The origin of this transition is attributed to subsequent vertical phase separation, with PFB wetting the substrate/film interface or film/vapor interface or both. In addition to the mechanisms of phase separation, the implications of the observed morphology changes for device performance are also discussed.

Introduction

Solution-processing of conjugated polymer blends is a convenient way to produce thin, two-component organic semiconducting layers for optoelectronic device applications such as polymer light-emitting diodes (LEDs) and solar cells.[1,2] Of the two polymers that comprise the blend, one polymer (or often in the case of organic solar cells a fullerene derivative[3]) acts as an electron transporter while the other acts as a hole transporter. Efficient operation relies upon the formation of interconnected networks for efficient charge transport and/or charge separation that are produced as the two components phase separate. As the process of phase separation is highly complex,[4] a better understanding of the way in which polymers, in particular conjugated polymers, phase separate is crucial for understanding and optimizing device performance.

Blends of polyfluorenes have attracted a lot of interest as the active layer in efficient light-emitting diodes[5] and as a model system for studying the influence of morphology on photovoltaic performance.[6−8] In these blends, the polymer poly(9,9′-dioctylfluorene-*co*-benzothiadiazole) or F8BT is used as the electron-transporting polymer while either poly(9,9′-dioctylfluorene-*co*-bis-*N,N*′-(4,butylphenyl)-bis-*N,N*′-phenyl-1,4-phenylenediamine) (PFB) or poly(9,9-dioctylfluorene-*co*-*N*-(4-butylphenyl)diphenylamine) (TFB) is used as the hole-transporting polymer in solar cells and LEDs, respectively. Blends of both F8BT with PFB and F8BT with TFB are observed to exhibit similar morphological characteristics.[9,10] In particular, when spin-coating such blends from high boiling point solvents such as xylene, a mesoscale lateral phase separation is produced. This laterally phase-separated morphology is complex, adding further challenge to the interpretation of device operation. In addition to the lateral phase separation, there is evidence for additional vertical segregation, with the hole transporting polymer, either PFB or TFB, forming a wetting layer at the substrate/film interface[9,11] and a partial capping layer at the film/air interface.[9,12] Furthermore, as observed by Raman microscopy,[13] and more recently by high-resolution X-ray spectromicroscopy,[10] the domains are not pure, with the observation of an enriched interfacial region in the F8BT phase.[14] Thus, in the case of TFB/F8BT LEDs, the bright emission that is observed near the mesoscale domain interfaces[5] may be explained in terms of either efficient electron−hole capture at the domain interfaces[5] or efficient electron injection and transport through F8BT-rich interfacial regions[14] with electron−hole recombination at the interface with the TFB-rich wetting layer.[9]

For the case of solar cell operation, it was similarly thought that charge collection would be most efficient near interface regions, with efficient exciton dissociation at the domain interfaces followed by efficient charge transport through the respective hole-transporting or electron-transporting domains.[15] Indeed, a linear correlation between interfacial area and device external quantum efficiency (EQE) was observed for blends where the degree of phase separation has been varied by varying either weight ratio,[15] molecular weight,[16] or film drying time.[17] However, direct microscopy studies that locally probe either photocurrent generation efficiency[18] or photoinduced charging rates[8] have concluded that the centers of the mesoscale domains and not their interfaces are responsible for the majority of photocurrent. These results are supported by prior STXM results that show that the centers of these mesoscale domains are in general not pure but exhibit variations in domain purity that can account for variations in device efficiency.[10] Similar studies have been carried out characterizing the influence of the morphology of polymer/fullerene composites on solar cell

* Corresponding author: e-mail crm51@cam.ac.uk, Tel +44 (0)1223 337285, Fax +44 (0)1223 764515.
† University of Cambridge.
‡ North Carolina State University.
§ University of Newcastle.
⊥ Present address: Swiss Light Source, Paul Scherrer Institut, Villigen, 5232 Switzerland.
∥ Australian Synchrotron.

10.1021/ma801816r CCC: $40.75
Published on Web 04/14/2009

performance;[19−23] however, polymer/fullerene blends, being comprised of a polymer and a C_{60} derivative, are likely to display different phase separation dynamics compared to all-polymer blends.[24,25]

While significant progress has been made in understanding how these phase-separated structures affect device performance, the mechanism of their formation still remains to be fully understood. In general, in the bulk phase separation proceeds either by the nucleation and growth of one phase in a surrounding phase or by the process of spinodal decomposition.[26] In the former case, phase separation relies on the formation of a droplet of the minority phase to act as a seed for nucleation, although in some circumstances (notably polymer/fullerene blends) the majority phase nucleates.[27] For a system with an evaporating solvent, this process may be seeded when the polymer with lower solubility begins to precipitate out of solution or forms a gel. For the case of spinodal decomposition, phase separation is delayed until the system enters an unstable region of the phase diagram whereby a small fluctuation in composition lowers the free energy and phase separation proceeds immediately by the amplification of random composition fluctuations.[26] For blends of TFB and F8BT Kim et al. proposed a model whereby phase separation proceeds via spinodal decomposition for blends with an equal blend ratio and by nucleation and growth for blends with a significantly unbalanced blend ratio.[9] However, the conditions under which phase separation proceeds during the process of spin-coating differ significantly from bulk conditions in which spinodal decomposition and nucleation and growth are traditionally described. In particular, the substrate/film and film/air surfaces break the symmetry and can impose a direction on phase separation. This can lead to the formation of wetting and capping layers that form in competition with bulk phase separation. Indeed, through the use of surface modification and a very high boiling point solvent (isodurene) Arias et al. reported a complete vertical phase separation of PFB and F8BT blends.[28] Furthermore, Heriot and Jones have recently proposed that laterally phase-separated features in spin-coated thin film polymer blends may actually proceed via an initial, transient wetting layer.[29] Under this mechanism, the film first separates into two layers which is followed by an instability of the polymer/polymer interface that grows until the magnitude of the instability is such that the internal liquid−liquid interface meets the surface at which point the film laterally phase separates.[29] This interfacial instability mechanism has been reported for 50:50 blends (by weight) of polystyrene and poly(methyl methacrylate)[29] as well as for 56:44 blends of PFB and F8BT.[30] Thus, the substrate/film and film/air interfaces play an important role in the phase separation of polymer thin films formed by spin-coating, with the classical, bulk descriptions not necessarily valid.

To gain a better understanding of the evolution of phase separation in conjugated polymer thin films not only during casting but also upon further processing, we have employed X-ray spectromicroscopy (or STXM)[31] to study PFB:F8BT films of different weight ratios and with controlled degrees of phase separation. Film coating has been carried out in a solvent-saturated atmosphere that slows the evaporation rate allowing for the evolution of phase separation to proceed beyond typical spin-coated structures. Furthermore, by varying the time spent in this solvent-saturated atmosphere, the dynamics of phase separation can be observed. Predicting the thermodynamic equilibrium structures toward which the morphology normally evolves is complicated for the PFB:F8BT:*p*-xylene system, as the solvent modifies the interfacial energies at the polymer/substrate interface, the polymer/polymer interface, and the polymer/vapor interface. Utilization of interfacial and surface energies and solubility parameters[9,25] alone is insufficient; the solvent/substrate and polymer/substrate interfacial energies must also be known. This peril can be appreciated by considering that even in the presence of a selective solvent for polystyrene (PS), a PS adsorption layer is formed on a poly(methyl methacrylate) substrate.[32] Furthermore, the morphological evolution observed under the conditions relevant to device structure formation might be entirely limited by kinetics as the F8BT phase will likely form a gel or highly viscous phase.[9] It is because of these difficulties that a heuristic approach based on advanced characterization is warranted. While the morphology of polymer blends has typically been evaluated by atomic force microscopy (AFM), X-ray spectromicroscopy utilizes near-edge X-ray absorption fine-structure spectroscopy (NEXAFS) to measure the vertically integrated (bulk) chemical composition with a comparable spatial resolution. Thus, we are able to observe the evolution of not only the structures of these blends but also the internal chemical composition of the phases, providing new insight into the dynamics of phase separation in these materials.

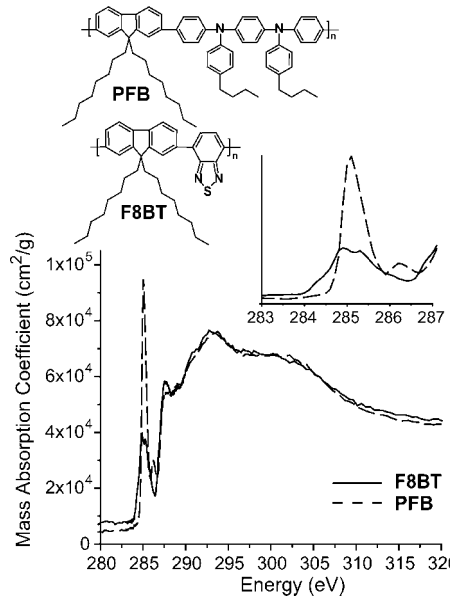

Figure 1. Chemical structures and NEXAFS spectra of pristine films of PFB and F8BT. The inset shows an expanded region around the π^* absorption peak highlighting the differences in the X-ray absorption spectra of these materials at these energies.

Experimental Details

Materials. Poly(9,9′-dioctylfluorene-*co*-bis-*N,N*′-(4,butylphenyl)-bis-*N,N*′-phenyl-1,4-phenylenediamine) (PFB) and poly(9,9′-dioctylfluorene-*co*-benzothiadiazole) (F8BT) were supplied by Cambridge Display Technology Ltd. The molecular weights (M_W) and polydispersities were 135 000 and 2.3 for PFB and 151 000 and 2.4 for F8BT, respectively. Chemical structures of these two polymers are presented in Figure 1.

Sample Preparation. Blend solutions were prepared by dissolving each polymer separately in *p*-xylene and then mixing these respective solutions to give the desired weight ratio. Weight ratios of 5:1, 1:1, and 1:5 PFB:F8BT were used, with a total solution concentration of 17 g/L employed for all solutions. All films were prepared on oxygen plasma-treated glass slides, floated off onto deionized water, picked up with copper transmission electron microscopy (TEM) grids for STXM analysis, and transferred to a nitrogen glovebox to dry. Films were prepared either by spin-coating in ambient conditions or in a controlled atmosphere using the apparatus of Shikler et al.[17] This apparatus allows for spin-coating to proceed in a solvent-saturated atmosphere that slows the evaporation rate and allows for phase separation to proceed to different degrees while keeping the initial point on the phase

diagram constant. For films spin-coated in ambient conditions, the films were spin-coated until dry (typically less than 40 s). Films prepared in the solvent saturated environment were initially spun for 1 s only to spin off the majority of the solution with the film and then allowed to evolve in the solvent-saturated environment for a fixed time, typically between 1 and 6 min. After the prescribed time, the films were removed from the solvent-saturated environment and allowed to dry in ambient conditions. Spin speeds employed were 1500 rpm for 5:1 PFB:F8BT films, 2000 rpm for 1:1 PFB:F8BT films, and 2500 rpm for 1:5 PFB:F8BT films. The different spin speeds compensated for the variations in solution viscosity to produce final films of similar thickness. Films spin-coated in ambient conditions were measured to be only slightly thinner than those prepared with a more evolved morphology in the solvent-saturated atmosphere, presumably as the majority of the solvent is expelled from the substrate during the first 1 s of spin-coating. In particular, 5:1 PFB:F8BT films prepared in ambient conditions were measured to have a thickness of 100 ± 3 nm compared to 130 ± 30 nm for films produced in the saturated atmosphere; 1:1 PFB:F8BT films prepared in ambient conditions had a thickness of 95 ± 20 nm compared to 110 ± 30 nm for films produced in the saturated atmosphere; and 1:5 PFB:F8BT films prepared in ambient conditions had a thickness of 92 ± 5 nm compared to 105 ± 5 nm for films produced in the saturated atmosphere. Pristine films of PFB and F8BT with known thickness (80 ± 3 and 100 ± 2 nm, respectively) were also prepared for measurement of reference NEXAFS spectra and to provide thickness calibration for the STXM images of the blend films. All film thicknesses were measured with a Dektak 6 M profilometer. AFM imaging was also performed on samples prior to float off, using a Digital Instruments Nanoscope IIIa in noncontact mode.

STXM Measurements. X-ray microscopy measurements were performed at beamline 5.3.2 of the Advanced Light Source at the Lawrence Berkeley National Laboratory, California.[33] Details of the experiment and data analysis can be found at length in our previous publications.[10,14] STXM utilizes differences in the NEXAFS spectra of the constituent materials to provide chemical contrast, with spatial resolution provided by focusing the monochromated X-rays with a Fresnel zone plate to a spot size of 50 nm or less. The TEM grid-mounted samples are rastered with respect to the incident beam to produce X-ray absorption images. Used in conjunction with a synchrotron beamline fitted with a high-resolution monochromator, the probing X-ray beam can be tuned to near-edge absorption resonances that are characteristic of the molecular structure of a particular material, thereby providing chemical sensitivity and selectivity. By observing X-ray absorption as a function of X-ray energy, NEXAFS spectra may also be taken at specific points of interest, along a line or indeed over a given area. Combining X-ray absorption images acquired at two or more energies (at which there is a difference in the X-ray absorption of the two materials) with knowledge of the NEXAFS spectra of reference component films is sufficient for quantitative compositional maps of the blend films to be produced. However, X-ray absorption images were acquired at several energies (280.0, 284.7, 285.1, and 320.0 eV) to provide additional energies for a better quantitative fit. Furthermore, full NEXAFS spectra were sampled from selected regions of each image and fitted to a sum of the pristine spectra. The results from this spectral fitting were then used as a cross-check for the results of the image analysis. It should be noted that thickness variations in the sample are automatically accounted for by the analysis, since measurement of the X-ray optical density at chemically insensitive energies (e.g., 320 eV) of the pure films of known thickness provides for an absolute thickness calibration. Image analysis was assisted by use of the IDL widget aXis2000 (http://unicorn.mcmaster.ca/aXis2000.html). For full details of our data analysis, please refer to our previous publication.[14]

Results and Discussion

Figure 1 presents the chemical structures and X-ray absorption spectra of pristine films of PFB and F8BT. While the two

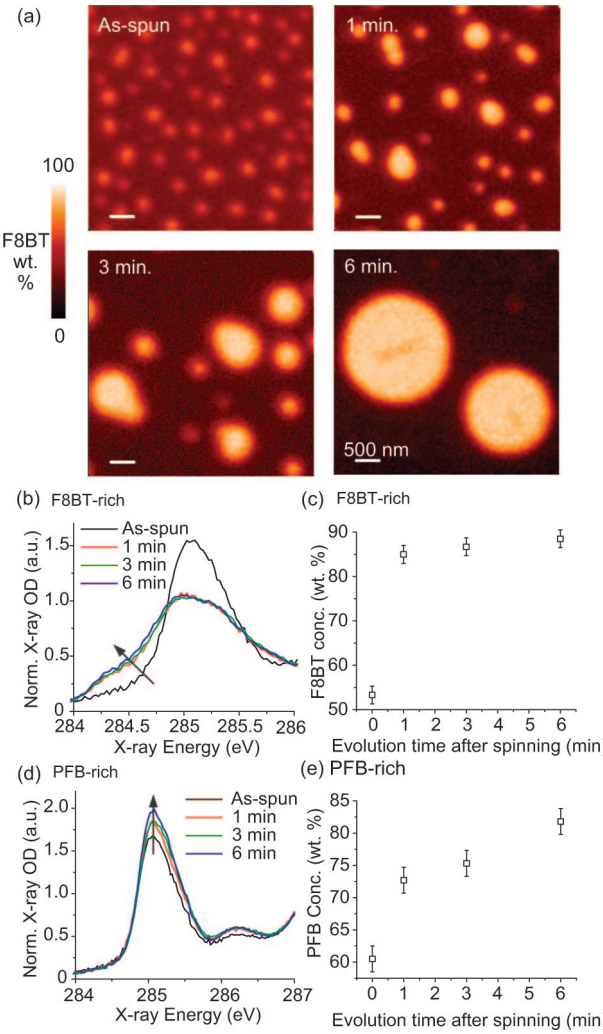

Figure 2. Evolution of the morphology of films with a weight ratio of 5:1 PFB:F8BT: (a) STXM images; (b, d) normalized NEXAFS spectra of F8BT-rich and PFB-rich domains, respectively; (c, e) concentrations for the F8BT-rich domain and PFB-rich domains, respectively, determined by least-squares fitting of blend spectra with a sum of pristine spectra.

polymers have similar absorption spectra above ~287 eV, corresponding to transitions from 1s to σ^* states, the absorption spectra between 284 and 287 eV corresponding to 1s to π^* transitions are markedly different, providing the basis for chemical contrast and quantitative analysis. As shown in the inset to Figure 1, the π^* spectrum of F8BT is characterized by a broad, multicomponent peak with a low-energy shoulder (onset at 284 eV), while PFB has a narrower, more intense peak at 285.1 eV.

Figure 2 presents X-ray microscopy images of a series of 5:1 PFB:F8BT blends along with NEXAFS spectra and plots of component fits for PFB-rich and F8BT-rich domains. From the STXM images it can be clearly seen that the size of the enclosed F8BT-rich domains systematically grows as the time in the solvent-saturated atmosphere increases from 1 to 6 min. Additionally, F8BT-rich spots can be seen to coalesce in the 1 and 3 min films. Examining the NEXAFS spectra of the PFB and F8BT domains (Figure 2b,d, respectively) and the corresponding component concentrations (Figure 2c,e, respectively), it can be seen that the purity of both PFB-rich and F8BT-rich domains systematically increases as the process of phase separation evolves. In the as-spun film, the F8BT-rich spots are measured to have a concentration of only 53% F8BT, consistent with previous observations.[10,14] The F8BT concentration of this phase dramatically increases to 85% when the film is left in

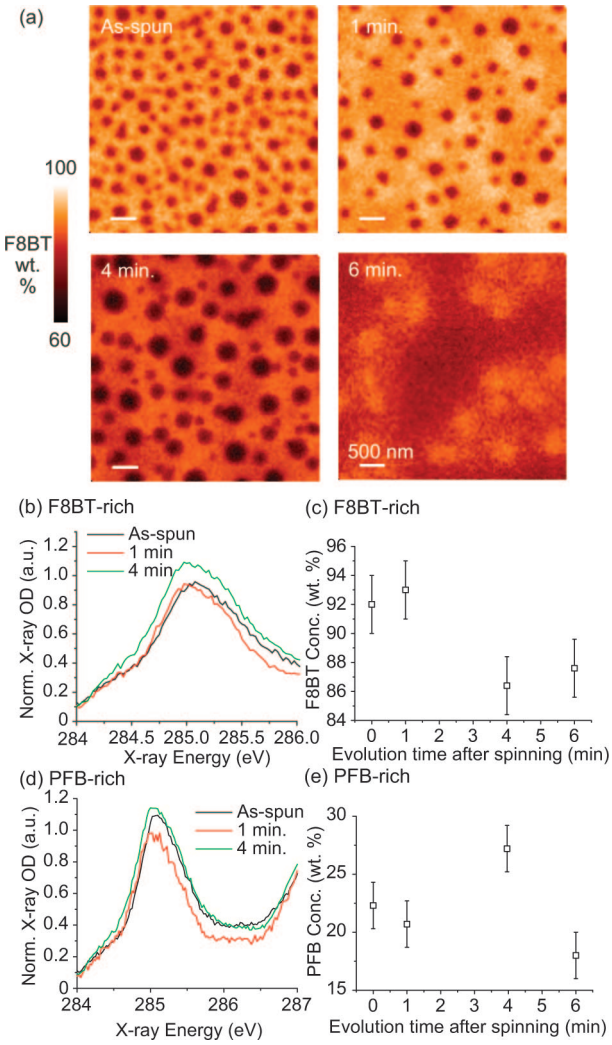

Figure 3. Evolution of the morphology of films with a weight ratio of 1:5 PFB:F8BT: (a) STXM images; (b, d) normalized NEXAFS spectra of F8BT-rich and PFB-rich domains, respectively; (c, e) fitted apparent concentrations for the F8BT-rich domain and PFB-rich domains, respectively.

the solvent-saturated atmosphere for 1 min and further increases to nearly 90% F8BT as phase separation continues. Similarly, the purity of the PFB-rich phase systematically increases with increasing drying time, providing direct evidence that there is flow of material across the mesoscale domain boundary during phase separation. Interestingly, the apparent purity of the F8BT spots appears to saturate at around 90%, suggesting either some degree of residual PFB in near-equilibrium phases or, since STXM samples through the entire film averaging the effects of vertical phase separation, the presence of a wetting layer or capping layer of PFB. The apparent purity of the PFB-rich phase on the other hand does not appear to have reached an equilibrium concentration after 6 min. This suggests that the F8BT chains have a lower mobility than PFB and/or that F8BT has a higher miscibility in PFB than PFB in F8BT. The former can be readily understood, given that PFB is more soluble in *p*-xylene than F8BT.[25]

Figure 3 presents the evolution of phase separation in 1:5 PFB:F8BT blends. Unlike the evolution of the 5:1 PFB:F8BT blend, we do not observe a gradual evolution in the composition of the phases in 1:5 blends from as-spun to the 4 min evolved film, with the F8BT-rich phase showing a similar concentration to the as-spun films. In contrast to this essentially arrested morphology observed at shorter evolution times, there is a dramatic change in morphology from 4 to 6 min with an

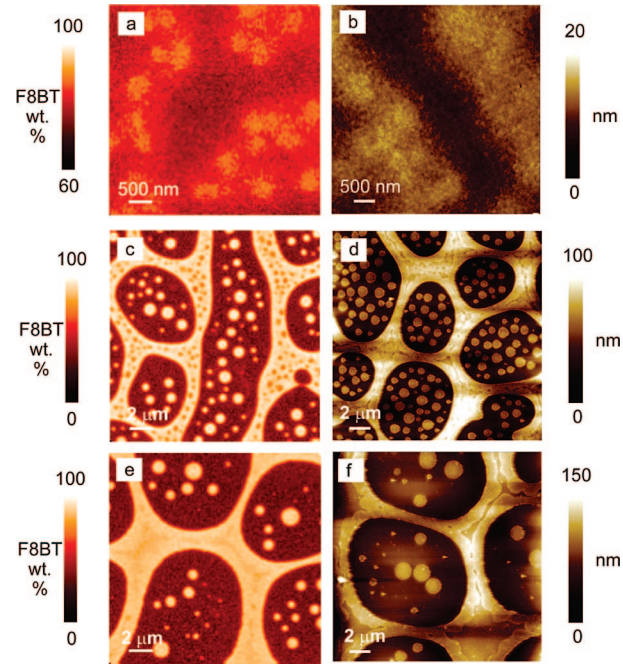

Figure 4. Comparison of X-ray microscopy images (a, c, e) and atomic force microscopy images (b, d, f): (a) and (b) are of a 6 min evolved 1:5 PFB:F8BT film; (c) and (d) are of a 3 min evolved 1:1 PFB:F8BT film; and (e) and (f) are of a 6 min evolved 1:1 PFB:F8BT film.

apparent phase inversion characterized by the disappearance of enclosed PFB-rich phases and the appearance of segregated F8BT-rich regions. The driving force for this dramatic change could be the segregation of PFB to the substrate similar to what has been previously observed in the TFB:F8BT system[9] and F8 in the F8:F8BT system.[11] At the same time, the better solubility of PFB in *p*-xylene would favor a PFB-rich layer to form at the polymer−vapor interface. Comparing STXM and AFM images (Figure 4), the F8BT-rich regions in the 6 min evolved 1:5 film correspond to raised regions on the film surface, suggesting at least an incomplete PFB surface layer. Whatever the reason, the STXM microscopy clearly indicates that this change in morphology has to be a transition from a predominantly 2D structure to a more layered structure, with further experiments planned to directly measure and map surface composition. Our observation of vertical phase stratification following lateral phase separation is in principle opposite to the mechanism proposed by Heriot and Jones whereby lateral phase separation is preceded by a vertical phase separation.[29] Of course, the time scales at which these mechanisms are at work (a few seconds compared to a few minutes) are very different for the two mechanisms. Additionally, we observe lateral phase separation preceding vertical phase separation for a blend system with an unbalanced blend ratio.

Figure 5 presents X-ray microscopy images of the evolution of phase separation in 1:1 PFB:F8BT blends. While more complicated, the evolution of 1:1 PFB:F8BT films shares features in common with the evolution of both 5:1 and 1:5 PFB:F8BT films. The STXM images show that both PFB-rich and F8BT-rich phases in the 1:1 blend increase in size with increasing drying time as well as the size and purity of the F8BT spots enclosed within the PFB-rich phase, similar to what is observed for the 5:1 blend. An enclosed PFB-rich phase is also observed in the F8BT-rich phase of the 3 min evolved film, which "disappears" after a further 3 min similar to the dynamics observed for the 1:5 PFB:F8BT blend. Despite these similarities, there are some apparent quantitative discrepancies between the evolution of the 1:1 PFB:F8BT blend compared to the other blends discussed above. In particular, neither F8BT-rich nor

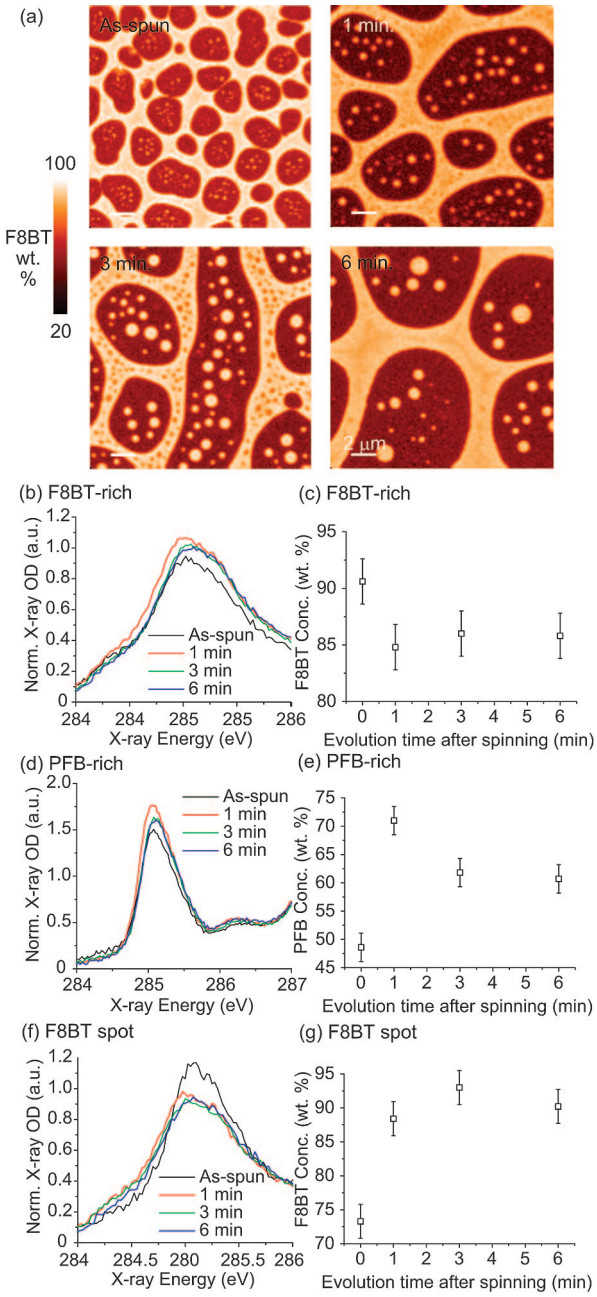

Figure 5. Evolution of the morphology of films with a weight ratio of 1:1 PFB:F8BT: (a) STXM images; (b, d, f) normalized NEXAFS spectra of the F8BT-rich domain, PFB-rich domain and F8BT spots, respectively; (c, e, g) fitted concentrations for the F8BT-rich domain, PFB-rich domain and F8BT spots, respectively.

PFB-rich primary domains show a systematic increase in purity with drying time. For example, the F8BT-rich domain appears to be already quite pure in the spin-coated film with a measured concentration of more than 90% F8BT, with the apparent purity of the more evolved domains slightly less at 85% F8BT. This observation of very pure F8BT-rich domains in spin-coated films suggests that the mechanism leading to the initial lateral phase separation is different than the subsequent phase separation process where the lateral domains grow in size as observed here by STXM. The initial process of lateral phase separation may be conveniently described by the initial vertical phase separation mechanism proposed by Jones et al.[29]

Examining the PFB-rich domain near F8BT domain walls in the evolution of the 1:1 PFB:F8BT blend reveals a depletion of F8BT spots providing evidence that F8BT spots are lost from the PFB-rich domain to the F8BT-rich domain through Ostwald

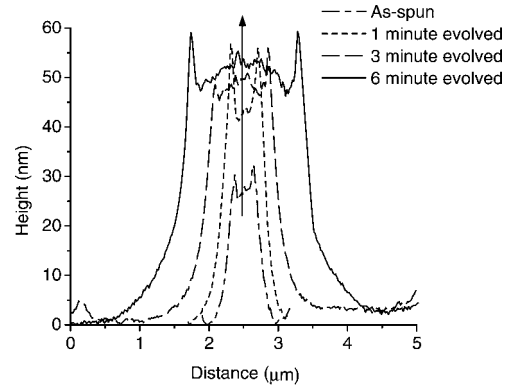

Figure 6. AFM cross sections of the height of the F8BT-rich phase in 5:1 PFB:F8BT blends.

ripening. Evidence for Ostwald ripening is present to a lesser degree in the F8BT-rich phase, perhaps due to the PFB-rich spots being kinetically trapped in the more viscous F8BT-rich phase. The complete "disappearance" of all of the PFB-rich spots in the F8BT-rich phase as the morphology evolves from the 3 min evolved film to the 6 min evolved film may also be seen as evidence for the draining of these PFB-rich spots into the underlying PFB-rich wetting layer, or to a PFB capping layer, similar to the evolution of the 1:5 PFB:F8BT film. Comparing STXM and AFM images (Figure 4), the PFB minority phase can just be distinguished in the AFM image of the 3 min evolved film, along with the terrace at the edge of the F8BT domain bounding a partial PFB capping layer as identified by scanning Kelvin probe measurements.[12] In Figure 4e,f, which compares STXM and AFM images of the 6 min evolved 1:1 film, the PFB minority phase can no longer be seen, yet the structure of the PFB capping appears unchanged. Interestingly, the structure of the partial PFB capping layer on the F8BT phase may be explained by the presence of a PFB-rich surface layer during vapor exposure (and during the early stages of spin-coating) that dewets when the vapor is removed (or when then solvent evaporates). The formation of such a PFB-rich surface layer would be favored given the solubility parameters of PFB (9.5 $(cal/cm^3)^{1/2}$), F8BT (10.0 $(cal/cm^3)^{1/2}$), and xylene (8.8 $(cal/cm^3)^{1/2}$).[25] Additional evidence for a PFB capping layer that dewets during drying is seen in the roughness of the surface of the F8BT-rich spots in the 5:1 blend (see Figure 6) with sharp spikes at the edge of the domains. Further experiments are planned to directly measure and map the surface compositions of PFB/F8BT blends to shed more light on this issue. Clearly, any additional vertical phase separation in addition to the lateral phase separation that is more readily quantified by STXM will make interpretation of the STXM data more challenging and may help to explain the more complicated compositional trends observed for the 1:1 and 1:5 blends.

The results presented here have implications for the interpretation of photovoltaic device data.[15,17] While we do not present fresh device data here, the performance of devices based on PFB:F8BT films prepared in an saturated atmosphere with similar morphologies has been reported previously.[17] In particular, we note that not only does the mesoscale interfacial area decrease as the morphology coarsens,[15,17] but the internal domain composition also changes. The observed increase in domain purity, as observed for the 5:1 PFB:F8BT blend, will have a negative impact on photovoltaic device performance due to a decrease in exciton dissociation efficiency, evidenced by an increase in photoluminescence efficiency.[17] Thus, the observed decrease in photovoltaic device efficiency as morphology evolves can be accounted for by changes in photocurrent generation from within the domain centers due to a change in bulk composition and/or changes in nanoscale phase separa-

tion.[10] We also note that the height of the F8BT phase increases as the morphology evolves, as demonstrated by the AFM cross sections in Figure 6. (Note that while the height of the F8BT domain is measured relative to the top of the PFB phase, the STXM data show that the decrease in PFB domain height with morphological evolution is not as significant as the height increase shown in Figure 6.) Assuming that the F8BT-rich domain is more efficient at generating photocurrent, as observed by Coffey and Ginger and consistent with an optimum local blend ratio of 75% F8BT,[34] this increase in domain thickness will also negatively impact device performance. In particular, since the efficiency of this class of device is limited primarily by geminate recombination[35,36] with a strong electric field dependence of charge separation efficiency,[37] the increased domain height in more evolved films will decrease the internal electric field, reducing charge separation efficiency and hence overall device efficiency.

Conclusions

We have used scanning transmission X-ray microscopy to study the evolution of phase separation in PFB:F8BT blends. For 5:1 blends, the evolution of the morphology is consistent with nucleation and growth, with both phases becoming purer as the film drying time increases. The F8BT-rich domains are observed to grow both by the flow of material across the mesoscale domain interface and through the coalescence of F8BT spots. For both 1:1 and 1:5 blends a more complicated evolution of morphology is observed. For the case of 1:5 blends, we found evidence for vertical stratification that follows the initial lateral phase separation, facilitated through a wetting of either the film/substrate or vapor/film interface. For the case of 1:1 blends, we have observed the evolution of secondary phase separation within both the F8BT-rich and PFB-rich domains. The evolution of F8BT-rich droplets in the PFB-rich domain mirrors the evolution of the morphology in 5:1 blends with these droplets becoming purer with increased evolution time. In the F8BT-rich domain, the PFB-rich minority phase also appears to drain into either a capping or wetting layer. We have also observed that the F8BT-rich phase is already very pure in as-spun films, suggesting that the initial phase-separation mechanism is different from the subsequent evolution of morphology observed here. We describe the initial lateral phase separation formation in terms of the model of Jones et al. which proceeds via an initial vertical phase separation. Finally, we have discussed the implications of our results for interpretation of photovoltaic performance, noting that increases in domain purity may explain the decrease in device efficiency with increased film drying time. Furthermore, the increase in F8BT domain height with drying time is also likely to affect the efficiency of charge separation leading to a further reduction in photovoltaic efficiency with morphological evolution.

Acknowledgment. The authors thank the ALS for beamtime and David Kilcoyne for technical assistance. This work was supported by the Engineering and Physical Sciences Research Council, U.K. (SUPERGEN IV), and by the Australian Research Council's Discovery funding scheme (DP0559417). We acknowledge financial support from the Commonwealth of Australia through the Access to Major Research Facilities Program. The ALS is supported by the Director, Office of Science, Office of Basic Energy Sciences, of the U.S. Department of Energy under Contract DE-AC02-05CH11231. Work at NCSU was supported by the U.S. Department of Energy under Grant DE-FG02-98ER45737. The authors also thank Cambridge Display Technology Ltd. for the supply of conjugated polymers used in this study. C. R. M. thanks Prof. Ullrich Steiner for helpful discussions.

References and Notes

(1) Moons, E. *J. Phys.: Condens. Matter* **2002**, *14*, 12235–12260.
(2) Veenstra, S. C.; Loos, J.; Kroon, J. M. *Prog. Photovoltaics* **2007**, *15*, 727–740.
(3) Yu, G.; Gao, J.; Hummelen, J. C.; Wudl, F.; Heeger, A. J. *Science* **1995**, *270*, 1789–1791.
(4) Bates, F. S. *Science* **1991**, *251*, 898–905.
(5) Morteani, A. C.; Dhoot, A. S.; Kim, J. S.; Silva, C.; Greenham, N. C.; Murphy, C.; Moons, E.; Ciná, S.; Burroughes, J. H.; Friend, R. H. *Adv. Mater.* **2003**, *15*, 1708–1712.
(6) Halls, J. J. M.; Arias, A. C.; MacKenzie, J. D.; Wu, W.; Inbasekaran, M.; Woo, E. P.; Friend, R. H. *Adv. Mater.* **2000**, *12*, 498–502.
(7) Kietzke, T.; Neher, D.; Kumke, M.; Montenegro, R.; Landfester, K.; Scherf, U. *Macromolecules* **2004**, *37*, 4882–4890.
(8) Coffey, D. C.; Ginger, D. S. *Nat. Mater.* **2006**, *5*, 735–740.
(9) Kim, J. S.; Ho, P. K. H.; Murphy, C. E.; Friend, R. H. *Macromolecules* **2004**, *37*, 2861–2871.
(10) McNeill, C. R.; Watts, B.; Thomsen, L.; Ade, H.; Greenham, N. C.; Dastoor, P. C. *Macromolecules* **2007**, *40*, 3263–3270.
(11) Higgins, A. M.; Martin, S. J.; J., T. R.; Chappell, J.; Voigt, M.; Lidzey, D. G.; Jones, R. A. L.; Geoghegan, M. *J. Phys.: Condens. Matter* **2005**, *17*, 1319–1328.
(12) Chiesa, M.; Burgi, L.; Kim, J.-S.; Shikler, R.; Friend, R. H.; Sirringhaus, H. *Nano Lett.* **2005**, *5*, 559–563.
(13) Stevenson, R.; Arias, A. C.; Ramsdale, C.; MacKenzie, J. D.; Richards, D. *Appl. Phys. Lett.* **2001**, *79*, 2178–2180.
(14) McNeill, C. R.; Watts, B.; Thomsen, L.; Belcher, W. J.; Greenham, N. C.; Dastoor, P. C. *Nano Lett.* **2006**, *6*, 1202–1206.
(15) Snaith, H. J.; Arias, A. C.; Morteani, A. C.; Silva, C.; Friend, R. H. *Nano Lett.* **2002**, *2*, 1353–1357.
(16) Snaith, H. J.; Friend, R. H. *Thin Solid Films* **2004**, *451−452*, 567–571.
(17) Shikler, R.; Chiesa, M.; Friend, R. H. *Macromolecules* **2006**, *39*, 5393–5399.
(18) McNeill, C. R.; Frohne, H.; Holdsworth, J. L.; Dastoor, P. C. *Nano Lett.* **2004**, *4*, 2503–2507.
(19) Hoppe, H.; Niggemann, M.; Winder, C.; Kraut, J.; Hiesgen, R.; Hinsch, A.; Meissner, D.; Sariciftci, N. S. *Adv. Funct. Mater.* **2004**, *14*, 1005–1011.
(20) Martens, T.; D'Haen, J.; Munters, T.; Beelen, Z.; Goris, L.; Manca, J.; D'Olieslaeger, M.; Vanderzande, D.; de Schepper, L.; Andriessen, R. *Synth. Met.* **2003**, *138*, 243–247.
(21) Shaheen, S. E.; Brabec, C. J.; Sariciftci, N. S.; Padinger, F.; Fromherz, T.; Hummelen, J. C. *Appl. Phys. Lett.* **2001**, *78*, 841–843.
(22) van Duren, J. K. L.; Yang, X.; Loos, J.; Bullie-Lieuwma, C. W. T.; Sieval, A. B.; Hummelen, J. C.; Janssen, R. A. J. *Adv. Funct. Mater.* **2004**, *14*, 425–434.
(23) Yang, X.; Loos, J.; Veenstra, S. C.; Verhees, W. J. H.; Wienk, M. M.; Kroon, J. M.; Michels, M. A. J.; Janssen, R. A. J. *Nano Lett.* **2005**, *5*, 579–583.
(24) Müller, C.; Ferenczi, T. A. M.; Campoy-Quiles, M.; Frost, J. M.; Bradley, D. D. C.; Smith, P.; Stingelin-Stutzmann, N.; Nelson, J. *Adv. Mater.* **2008**, *20*, 3510–3515.
(25) Nilsson, S.; Bernasik, A.; Budkowski, A.; Moons, E. *Macromolecules* **2007**, *40*, 8291–8301.
(26) Jones, R. A. L.; Richards, R. W. *Polymers at Surfaces and Interfaces*; Cambridge University Press: Cambridge, 1999.
(27) Yang, X.; van Duren, J. K. L.; Janssen, R. A. J.; Michels, M. A. J.; Loos, J. *Macromolecules* **2004**, *37*, 2151–2158.
(28) Arias, A. C.; Corcoran, N.; Banach, M.; Friend, R. H.; MacKenzie, J. D.; Huck, W. T. S. *Appl. Phys. Lett.* **2002**, *80*, 1695–1697.
(29) Heriot, S. Y.; Jones, R. A. L. *Nat. Mater.* **2005**, *4*, 782–786.
(30) Jukes, P. C.; Heriot, S. Y.; Sharp, J. S.; Jones, R. A. L. *Macromolecules* **2005**, *38*, 2030–2032.
(31) Ade, H.; Zhang, X.; Cameron, S.; Costello, C.; Kirz, J.; Williams, S. *Science* **1992**, *258*, 972–975.
(32) Harton, S. E.; Luning, J.; Betz, H.; Ade, H. *Macromolecules* **2006**, *39*, 7729–7733.
(33) Kilcoyne, A. L. D.; Tyliszczak, T.; Steele, W. F.; S., F.; Hitchcock, P.; Franck, K.; Anderson, E. H.; Harteneck, B. D.; Rightor, E. G.; Mitchell, G. E.; Hitchcock, A. P.; Yang, L.; Warwick, T.; Ade, H. *J. Synchrotron Radiat.* **2003**, *10*, 125–136.
(34) McNeill, C. R.; Abrusci, A.; Zaumseil, J.; Wilson, R.; McKiernan, M. J.; Halls, J. J. M.; Greenham, N. C.; Friend, R. H. *Appl. Phys. Lett.* **2007**, *90*, 193506.
(35) McNeill, C. R.; Westenhoff, S.; Groves, C.; Friend, R. H.; Greenham, N. C. *J. Phys. Chem. C* **2007**, *111*, 19153–19160.
(36) Yin, C.; Kietzke, T.; Neher, D.; Hörhold, H. H. *Appl. Phys. Lett.* **2007**, *90*, 092117.
(37) Marsh, R. A.; Groves, C.; Greenham, N. C. *J. Appl. Phys.* **2007**, *101*, 083509.

MA801816R